Received: 21 May 2024 | Revised: 22 August 2024 | Accepted: 23 August 2024

DOI: 10.1002/pamm.202400112

RESEARCH ARTICLE

Analysis and simulation of curved hoses under internal pressure—3D continuum models

Quirin Hoesch[1,2] | **Michael Roller**[1] | **Fabio Schneider-Jung**[1] | **Joachim Linn**[1] | **Ralf Müller**[2]

[1]Department of Mathematics for Vehicle Engineering, Fraunhofer Institute for Industrial Mathematics ITWM, Kaiserslautern, Germany

[2]Department of Civil and Environmental Engineering, Technical University of Darmstadt, Darmstadt, Germany

Correspondence
Quirin Hoesch, Department of Mathematics for Vehicle Engineering, Fraunhofer Institute for Industrial Mathematics ITWM, Fraunhofer Platz 1, 67663 Kaiserslautern, Germany.
Email: quirin.hoesch@itwm.fraunhofer.de

Abstract

This contribution aims to model and characterize the nonlinear elastic behavior of hoses under internal pressure. A highly resolved 3D continuum model is used to identify relevant effects of preformed hoses under internal pressure. The focus of this work is on the Bourdon effect, which is illustrated by simulating two simplified models, a full torus and a quarter torus. For a full torus, the Bourdon effect can be observed by the fact that the radius of curvature increases in addition to the expansion of the cross-sectional radius. For a quarter torus, which is a simplified example of a curved hose, the Bourdon effect can be observed by the tendency of the hose to straighten under internal pressure. Furthermore it is detected for both examples that the non-constant distribution of the poloidal (hoop) stress over the cross-section leads to an ovalization behavior. In addition, the model of a quarter torus is extended to a more complex model with straight hose sections at both ends.

1 | INTRODUCTION

Flexible structures, such as cables and hoses, are widely used in the automotive and heavy machinery industry [1]. Therefore a digital simulation tool, which is real-time capable and nevertheless physically correct, is required for the virtual safeguarding of these flexible structures. For this purpose, the structural-mechanical model and its mathematical formulation are crucial. It has been shown that Cosserat rod theory provides a suitable framework to model such flexible structures in a geometrically exact way [2]. However, when the hoses are preformed and subjected to internal pressure, a deformation behavior occurs that cannot be predicted easily using rod theory. Therefore, a 3D continuum model is used to reproduce the behavior of curved hoses under internal pressure. With such a model, we can investigate the dominant effects of the internal pressure for different kind of hoses and figure out, if we can include these effects in nonlinear rod theory. With our 3D solid continuum model, all known effects like pressure dependent bending stiffness, radial expansion, axial shortening, cross-sectional deformation, as well as a curvature dependent force, also known as the Bourdon effect, can be simulated [3]. We focus on the Bourdon effect, which is a dominant effect for the deformation behavior of curved hoses under internal pressure by simulating two illustrative models, a full torus and a quarter torus. Furthermore, the cross-sectional ovalization is shown in both examples and the relationship to the non-constant distribution of the

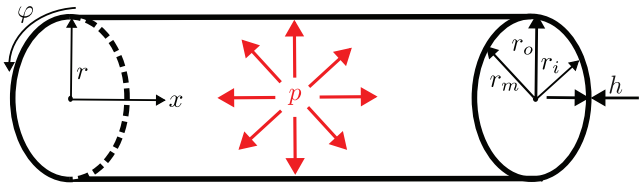

FIGURE 1 Geometry of a pressurized straight hose.

poloidal (hoop) stress in the cross-section is established. Moreover, the quarter torus model is expanded to incorporate straight hose sections at both ends to simulate the behavior of a hose system.

2 | ANALYTICAL CONSIDERATIONS

In this section, we present analytical considerations which are relevant for the description of the behavior of hoses. We give a brief introduction to already known effects of straight hoses. These are extended to curved hoses by presenting the Bourdon force. Furthermore, the stresses in a full torus are derived and the resulting ovalization of the cross-section is explained.

2.1 | Effects of straight pressurized hoses

Hoses are geometrically hollow, long, cylindrical structures. The straight hose is the simplest and best-studied case. Barlow's equation specifies the mechanical stresses in thin-walled, rotationally symmetrical bodies, which are subjected to internal pressure. As a membrane stress description, it is based on an equilibrium of forces, which means that neither deformation assumptions nor elasticity values are required for calculation.

For a straight hose with closed ends, the stresses are as follows:

$$\sigma_\varphi = \frac{p r_m}{h}; \quad \sigma_x = \frac{p r_m}{2h}; \quad \sigma_r(r_i) = -p; \quad \sigma_r(r_o) = 0, \tag{1}$$

with the cylindrical coordinates r-radial, φ-hoop, and x-axial and the internal pressure p, the wall thickness h, the outer resp. inner radius r_o and r_i, as well as the medium radius r_m, see Figure 1. The basic statement of Barlow's formula is that the hoop stress is twice the axial stress [4]. Basing on these stresses, the strains and thus the deformations can be determined by applying a constitutive law. For the example of a straight hose without end caps with an isotropic, linear elastic material with poisson-ratio $0 < \nu < 0.5$, it comes to a radial expansion due to the internal pressure, which leads to an axial shortening in consequence of the transverse contraction. The movement in the circumferential direction remains unaffected due to the rotational symmetry. Because of the radial expansion, the cross-section deforms and the wall thickness h decreases.

2.2 | Effects of curved pressurized hoses—The Bourdon effect

All the above mentioned effects also occur for curved hoses. An additionally known effect for curved hoses under internal pressure is a force pointing outwards which leads to a straightening of the hose. This effect is known since the 19th century as the Bourdon effect [5]. Every Bourdon pressure gauge works according to this principle. For the modeling of structures with a curved center line, a toroidal coordinate system is used with the three coordinate directions r-radial, θ-toroidal and φ-poloidal. The poloidal angle $\varphi = \frac{\pi}{2}$ is called extrados, $\varphi = \frac{3\pi}{2}$ is called intrados, while $\varphi = 0 = \pi$ is called crown, see Figure 2 [3]. In the following analytical considerations, due to the assumption of thin-walled structures, the radius r is used for the calculations and no distinction is made between r_o, r_i, and r_m.

In the following the Bourdon effect for a pressurized full torus is briefly recapitulated. Therefore, we calculate the outwardly directed effective force acting on an infinitesimal area dA of the torus by integrating the pressure p acting

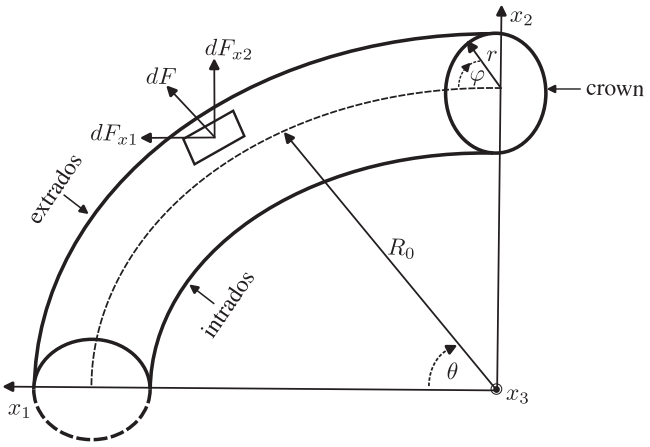

FIGURE 2 Outwardly directed force on an infinitesimal area of a curved hose with toroidal coordinates.

on dA. To derive the infinitesimal area dA of a torus, we use the toroidal angle θ and the poloidal angle φ, to convert Cartesian coordinates into toroidal coordinates. For a torus with a greater radius R_0 and a smaller radius r (see Figure 2) the parameterization is as follows

$$\begin{aligned} x_1(\theta,\varphi) &= (R_0 + r\sin\varphi)\cos\theta. \\ x_2(\theta,\varphi) &= (R_0 + r\sin\varphi)\sin\theta. \\ x_3(\theta,\varphi) &= r\cos\varphi. \end{aligned} \tag{2}$$

and

$$\vec{s} = x_1\vec{e_1} + x_2\vec{e_2} + x_3\vec{e_3}. \tag{3}$$

The area element dA follows from

$$dA = \left|\frac{\partial \mathbf{s}}{\partial\varphi} \times \frac{\partial \mathbf{s}}{\partial\theta}\right| d\varphi\, d\theta, \tag{4}$$

where $\times$ indicates the cross product. With the derivatives

$$\frac{\partial \mathbf{s}}{\partial\varphi} = \begin{pmatrix} r\cos\varphi\cos\theta \\ r\cos\varphi\sin\theta \\ -r\sin\varphi \end{pmatrix}, \quad \frac{\partial \mathbf{s}}{\partial\theta} = \begin{pmatrix} -(R_0 + r\sin\varphi)\sin\theta \\ (R_0 + r\sin\varphi)\cos\theta \\ 0 \end{pmatrix}, \tag{5}$$

an infinitesimal area dA of the torus can be described as follows

$$dA = r(R_0 + r\sin\varphi)d\varphi d\theta. \tag{6}$$

The force $\vec{dF}$, which acts on an infinitesimal area dA, results from the internal pressure p and can be decomposed into the components dF_{x1}, dF_{x2}, and dF_{x3} in the Cartesian system, see Figure 2:

$$dF = (pR_0 r + pr^2\sin\varphi)d\varphi d\theta; \quad dF_{x1} = dF\sin\varphi\cos\theta; \quad dF_{x2} = dF\sin\varphi\sin\theta; \quad dF_{x3} = dF cos\varphi. \tag{7}$$

By integrating the two Bourdon force components dF_{x1} and dF_{x2} along the cross section φ from 0 to 2π, we get the following:

$$\begin{aligned} F_{x1} &= \int_0^{2\pi}\int_{\theta_1}^{\theta_2} (pR_0 r + pr^2\sin\varphi)\sin\varphi\cos\theta d\varphi d\theta = \int_{\theta_1}^{\theta_2} pr\cos\theta d\theta \int_0^{2\pi} (R_0 + r\sin\varphi)\sin\varphi d\varphi \\ &= \int_{\theta_1}^{\theta_2} p\pi r^2\cos\theta d\theta. \end{aligned} \tag{8}$$

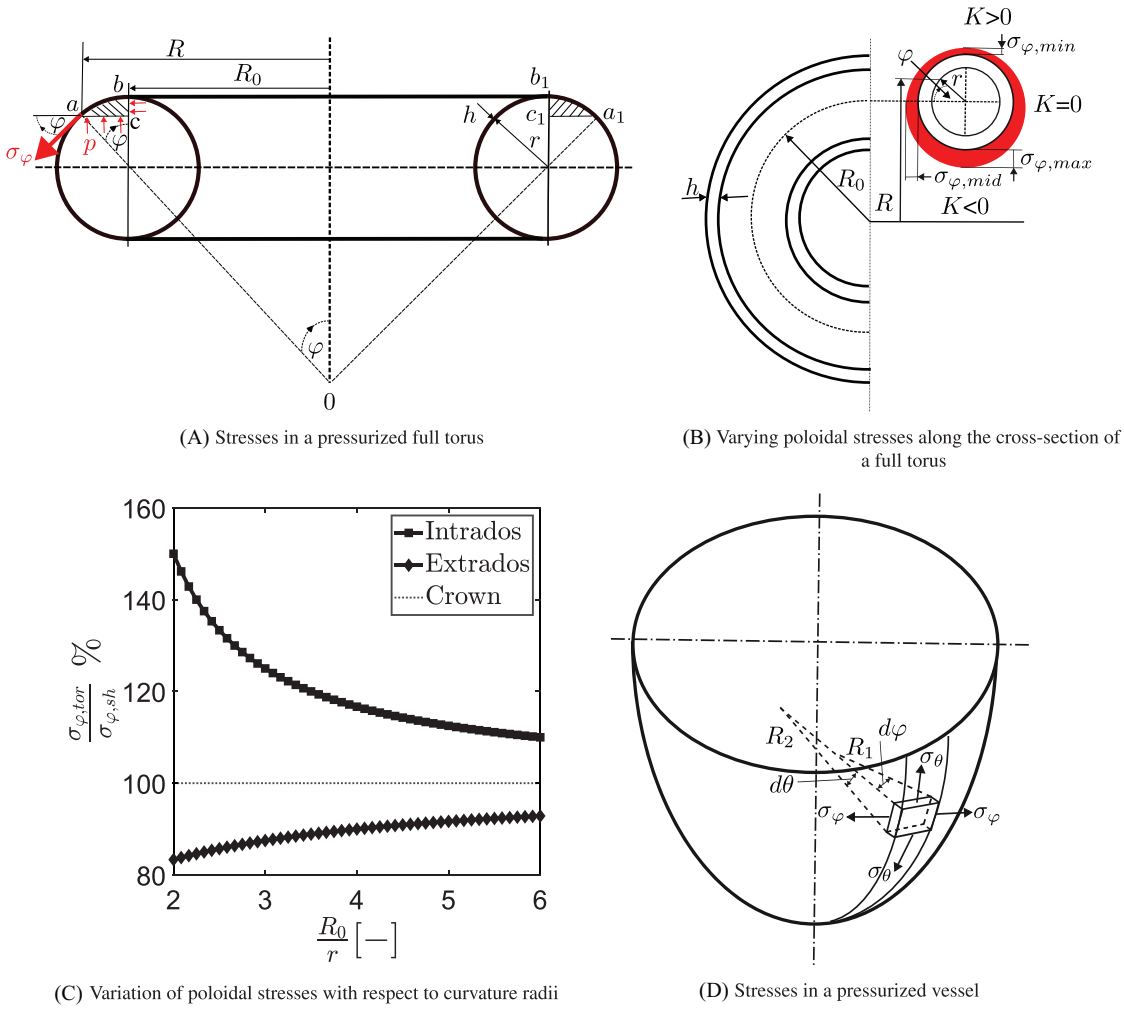

(A) Stresses in a pressurized full torus

(B) Varying poloidal stresses along the cross-section of a full torus

(C) Variation of poloidal stresses with respect to curvature radii

(D) Stresses in a pressurized vessel

FIGURE 3 Stresses in a full torus and in a general vessel.

$$F_{x2} = \int_0^{2\pi} \int_{\theta_1}^{\theta_2} (pR_0 r + pr^2 \sin\varphi) \sin\varphi \sin\theta d\varphi d\theta = \int_{\theta_1}^{\theta_2} pr \sin\theta d\theta \int_0^{2\pi} (R_0 + r\sin\varphi) \sin\varphi d\varphi$$
$$= \int_{\theta_1}^{\theta_2} p\pi r^2 \sin\theta d\theta. \tag{9}$$

F_{x1} and F_{x2} describe the effective force components acting on the torus fragment going from θ_1 to θ_2. The Bourdon force $F_{x1,2}(p, r, \theta)$ is consistent with an earlier study of Thiagarajan that proposed the same mathematical model [6]. The force component dF_{x3} does not depend on θ and disappears when being integrated along the cross-section φ from 0 to 2π, so that no Bourdon force appears in the x_3-direction.

2.3 | Ovalization

In this subsection, we take a closer look at the ovalization behavior which occurs when curved structures are subjected to pressure. For this purpose, we derive the stress distribution of a full torus under internal pressure, because it seems to differ from the stress distribution of a straight hose due to curvature effects. We assume again a membrane stress state, so that the internal pressure is always perpendicular to the inner wall and just normal stresses appear, which are assumed constant across the wall thickness. Figure 3A shows a cut through a pressurized full torus along the planes a–c and b–c. We see that balance occurs between the internal pressure acting on the annular plane a–c and the vertical component of

the poloidal stress σ_φ at point a.

$$\pi p(R^2 - R_0^2) = 2h\pi R \sin\varphi \sigma_\varphi \rightarrow \sigma_\varphi = \frac{p(R^2 - R_0^2)}{2hR\sin\varphi}. \tag{10}$$

The radius R describes the distance from the center plane to any point on the cross-section, which is point a, see Figure 3A. By inserting the relation $R = R_0 + r\sin\varphi$ in (10), we see that the poloidal stress depends on the poloidal angle φ, which varies along the circumference of the cross-section:

$$\sigma_\varphi = \frac{pr}{2h}\frac{2R_0 + r\sin\varphi}{R_0 + r\sin\varphi}. \tag{11}$$

By inserting different φ-values, we find a maximum poloidal stress value at the intrados $\varphi = \frac{3\pi}{2}$, while the minimum poloidal stress is at the extrados $\varphi = \frac{\pi}{2}$. Figure 3B shows the variation of the poloidal stress σ_φ around the cross-section of the torus. On the crown $\varphi = 0, \pi$, (11) reduces to the hoop stress in a straight cylinder, see Barlow's Equation (1).

$$\textbf{Min}: \ \sigma_\varphi(\frac{\pi}{2}) = \frac{pr}{2h}\frac{2R_0 + r}{R_0 + r}; \qquad \textbf{Max}: \ \sigma_\varphi(\frac{3\pi}{2}) = \frac{pr}{2h}\frac{2R_0 - r}{R_0 - r}; \qquad \textbf{Mid}: \ \sigma_\varphi(0,\pi) = \frac{pr}{h}. \tag{12}$$

In Figure 3C we see the variation of the maximum or minimum poloidal stress value of a full torus $\sigma_{\varphi,tor}$ in comparison with the hoop stress value of a straight hose $\sigma_{\varphi,sh}$. The stresses become larger for smaller curvature radii (torus with a small hole). The stresses at the intrados increase more pronounced than the stresses at the extrados decrease. The toroidal stress of a full torus can be calculated by the membrane stresses in a general vessel (see Figure 3D), where σ_θ is the longitudinal or meridional stress and σ_φ is the hoop stress in circumferential direction. The radius R_1 describes in Figure 3D the radius of curvature of the element in the hoop direction and the radius R_2 describes the meridional radius of curvature. Note that meridional and circumferential directions are perpendicular to each other. So the membrane stresses in a vessel are as follows [4]:

$$\frac{\sigma_\varphi}{R_1} + \frac{\sigma_\theta}{R_2} = \frac{p}{h}. \tag{13}$$

By modifying the principal radii of curvature of a general vessel to those of a torus, the principal radii R_1 and R_2 as well as their reciprocals, the principal curvatures K_1 and K_2, can be described as follows:

$$R_1 = r; \qquad R_2 = r + \frac{R_0}{\sin\varphi}; \qquad K_1 = \frac{1}{R_1} = \frac{1}{r}; \qquad K_2 = \frac{1}{R_2} = \frac{\sin\varphi}{R_0 + r\sin\varphi}. \tag{14}$$

This leads to the total Gauß-curvature of a torus, which is positive, negative or zero, depending on the angle φ (see Figure 3B):

$$K = K_1 K_2 = \frac{\sin\varphi}{r(R_0 + r\sin\varphi)}. \tag{15}$$

The toroidal stress σ_θ of a torus can now be calculated by the membrane stresses in a general vessel (13) using the radii of curvature of a torus (14). It is the same as for a straight cylinder (see Equation 1) and is thus constant and independent of position.

$$\frac{\sigma_\varphi}{R_1} + \frac{\sigma_\theta}{R_2} = \frac{p}{h} \rightarrow \frac{\sigma_\varphi}{r} + \frac{\sigma_\theta \sin\varphi}{R_0 + r\sin\varphi} = \frac{p}{h} \rightarrow \sigma_\theta = \frac{pr}{2h}. \tag{16}$$

Figure 4A shows the connection between the non-constant distributed poloidal stress σ_φ and the ovalization. As shown in Figure 3A, the poloidal stresses σ_φ balance the internal pressure p. If the principal axes a_1 and a_2 are of different length, the poloidal stresses differ as well and vice versa. For the case that the poloidal stresses of the main axis a_1 are greater than those of the main axis a_2, the length of axis a_1 is also greater than the length of a_2, resulting in longitudinal ovalization.

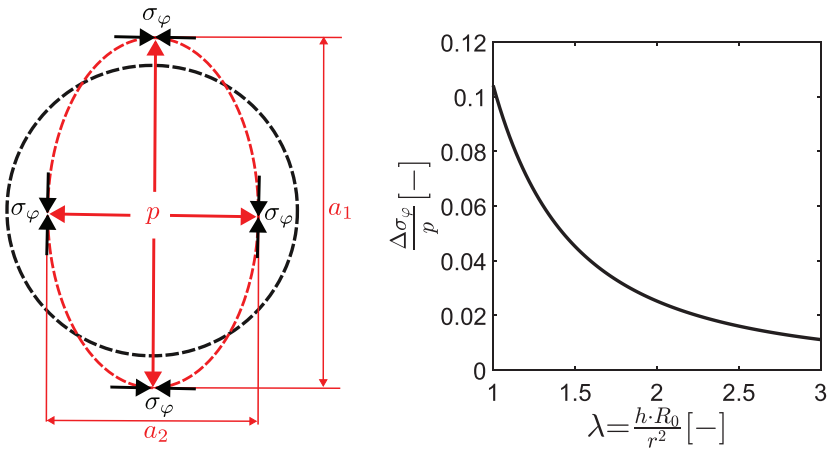

(A) Poloidal stress and ovalisation in the cross-section

(B) Poloidal stress factor over Kármán-factor

FIGURE 4 Poloidal stresses and ovalization in a full torus.

TABLE 1 Model parameters for finite element analysis.

Parameter	r_o	h	R_0	E	ν	p
Description	Outer radius	Thickness	Curvature radius	Young's modulus	Poisson-ratio	Pressure
Unit	(mm)	(mm)	(mm)	$(\frac{\text{N}}{\text{mm}^2})$	(-)	$(\frac{\text{N}}{\text{mm}^2})$
Value	12	2	50	750	0.4	1

Conversely, if the stresses at a_2 are higher than those at a_1, this leads to transversal ovalization. However, in the case of a torus, the poloidal stresses σ_φ at the ends of the longitudinal main axis a_1 are different, see (11), so that a new value $\Delta\sigma_\varphi$ is introduced to describe the ovalization behavior:

$$\Delta\sigma_\varphi = \frac{\sigma_{\varphi,max} + \sigma_{\varphi,min}}{2} - \sigma_{\varphi,mid}. \tag{17}$$

If $\Delta\sigma_\varphi \neq 0$, the originally circular cross-section ovalizes, depending on the stress values at the principal axes. The bigger $\Delta\sigma_\varphi$, the higher is the ovality Ω, which can be described by comparing the main axes a_1 and a_2:

$$\Omega[\%] = \frac{a_1 - a_2}{a_1 + a_2}. \tag{18}$$

A positive ovality value Ω means longitudinal ovalization, while a negative ovality value means transversal ovalization. In Figure 4B the dimensionless value $\frac{\Delta\sigma_\varphi}{p}$ is shown with respect to a geometrical factor $\lambda = \frac{hR_0}{r^2}$. This geometrical factor λ is normally used to describe the flexibility of pipe bends and was first introduced by Von Kármán [7]. It contains the curvature radius R_0, the radius r and also the wall thickness h. We observe that for lower λ, the ratio $\frac{\Delta\sigma_\varphi}{p}$ increases, so that consequently the ovality also increases. The narrower and thicker a curved hose becomes, the larger is the ovalization. The wider and thinner the geometry is, the smaller the ovalization.

3 | FINITE ELEMENT METHOD

To investigate the deformation behavior of pressurized, preformed hoses, we perform simulations with the finite element method using the commercial software ANSYS with its command language APDL [8, 9]. 3D continuum elements with hexahedron shape and 20 element nodes are used. A linear elastic, isotropic constitutive relation is applied. By implementing Large-Deformation Theory and defining the internal pressure p as a follower load, a quasi-static analysis via the Newton-Raphson-algorithm as solution method is performed. The model parameters are listed in Table 1.

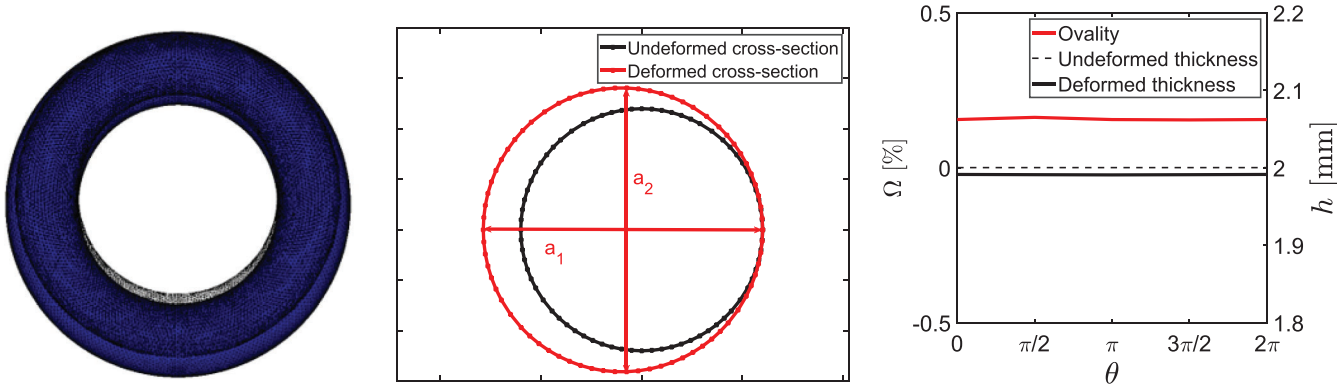

(A) Deformed vs. Undeformed structure

(B) Deformed vs. Undeformed cross-section

(C) Constant longitudinal ovalisation and thickness decrease over toroidal length θ

FIGURE 5 Full torus.

4 | RESULTS

In this section we verify the previously shown Bourdon effect (see Subsection 2.2) and the shown ovalization (see Subsection 2.3) with the finite element method (see Section 3). The results are presented for the examples of a full torus, a quarter torus and a combination of curved and straight hoses.

4.1 | Full torus

For a full torus, the Bourdon effect causes an increase in the radius of curvature R_0. The deformed structure is shown in Figure 5A, where it is constrained at one node with the coordinates $r = r_o$, $\theta = 0$, $\varphi = 0$ in the way $u^* = u_{r,\theta,\varphi} = 0$. Furthermore, we observe a radial expansion of the cross-section, as shown in Figure 5B. We define the principal axes, where a_1 is from extrados to intrados, while the axes a_2 is from crown to crown. We reveal a longitudinal ovalization behavior, which is explained in Subsection 2.3. The longitudinal ovalization Ω is constant and positive along the toroidal direction θ as shown in Figure 5C by the red line. Due to the radial expansion, the wall thickness h decreases constantly in toroidal θ-direction, represented by the solid black line and decreases also constantly in φ-direction. The dashed black line represents the undeformed thickness h of the full torus when not being pressurized.

4.2 | Quarter torus

The structural behavior of a pressurized quarter torus is shown. The Bourdon effect of this curved hose can be observed by the tendency to straighten under internal pressure. We use fixed-free displacement boundary conditions, where all nodes at $\theta = 0$ are constrained in the way $u^* = u_{\theta,\varphi} = 0$, while radial deformation is free. In Figure 6A, the finite element model is presented, whereas in Figure 6B, the deformed structure is shown with reference to the undeformed mesh. Looking at the deformed structure, the effect of straightening, while the cross section remains perpendicular to the toroidal axis, but rotates out of the cross-sectional plane, can be seen quite well. In Figure 6C, the ovalization behavior of the cross-section along the toroidal direction θ is shown. The inner radius of the quarter torus is described by the value r_i (black line), while r_m describes the mean radius (blue line) and r_o the outer radius (red line). The ovality values Ω are higher for the inner radius r_i than for the mean radius r_m and the outer radius r_o. This is because the deformation has a higher influence in percentage terms on smaller than on larger radii. Additionally, the ovality Ω is not constant over the toroidal direction θ and differs therefore from the ovalization of a full torus (see Figure 5C). This is due to the influence of the boundary conditions. At the free end of the quarter torus ($\theta = \frac{\pi}{2}$), the ovalization is zero due to the straightening behavior of the internal pressure. The radial deformation is permitted at the clamp ($\theta = 0$) and thus longitudinal ovalization occurs there. The highest ovalization does not occur in the toroidal center of the quarter torus ($\theta = \frac{\pi}{4}$), but about $\frac{1}{3}$ of the toroidal length of a quarter torus ($\theta = \frac{\pi}{6}$) and is also influenced by the boundary conditions.

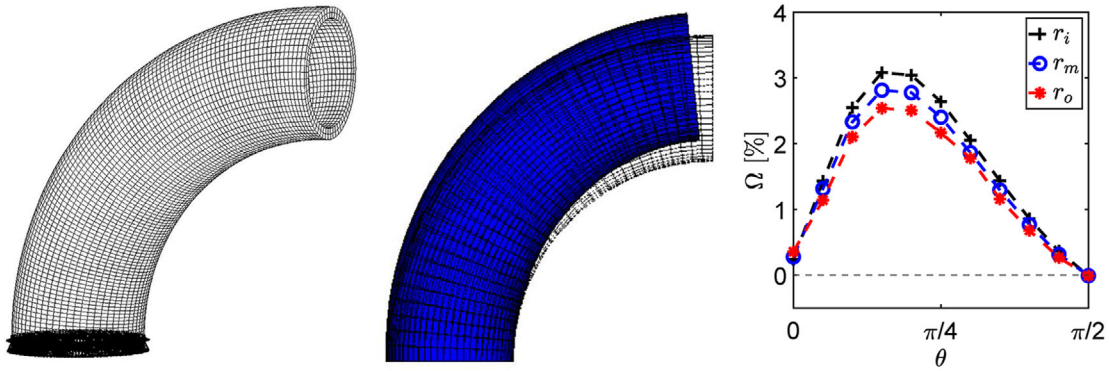

(A) Discretised Structure (B) Deformed Structure (C) Varying ovalisation over toroidal length θ

FIGURE 6 Quarter torus.

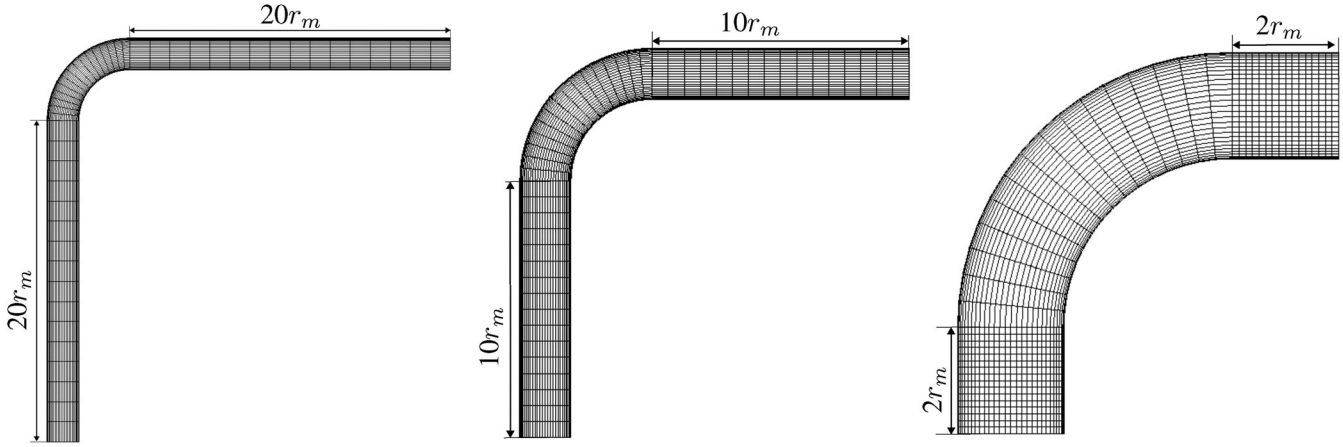

(A) Case a: Curved hose with connected straight hose with a length of $20r_m$ (B) Case b: Curved hose with connected straight hose with a length of $10r_m$ (C) Case c: Curved hose with connected straight hose with a length of $2r_m$

FIGURE 7 Geometry: Combination of curved and straight hoses.

4.3 | Combination of curved and straight hoses

Next, straight and curved hose sections are combined. For the geometry of the bend (R_0, r_o, h), the material (E, ν) and the pressure p, the same parameters from Table 1 are used. In Figure 6, the geometry of the discretized structure is shown for different straight lengths with 20, 10, and 2 times the mean cross-sectional radius r_m. The models are called case a, b, and c. At both ends, boundary conditions are applied using the cylindrical coordinate directions r, φ and x: $u^* = u_{\varphi,x} = 0$.

Figure 8A shows the deformed hose structure with a length of the straight hoses $20r_m$ (case a). A scaling factor of 20 was applied for better visualization. A closer look at the bend, which is the region of interest as the greatest stresses and deformations are expected there, shows that it resembles the deformation of a full torus. A stress analysis at the outer layer of the bend confirms the hypothesis that a curved hose with attached straight pieces behaves like a torus, see (11), (12), and (16) and the black lines in Figure 8B. All the stresses of the bend are θ-position independent. Therefore, the stresses are evaluated at the middle of the bend, see the red line Figure 8A. For case a (straight hose length $20r_m$), the radial and toroidal stress σ_r and σ_θ remain constant in the cross-section (black dashed lines), while the poloidal stress σ_φ varies and has its maximum at the intrados ($\varphi = \frac{3\pi}{2}$) and its minimum stress at the extrados ($\varphi = \frac{\pi}{2}$), see the black solid line in Figure 8B and Equation (12). According to previous studies [3, 10–12], the length of the attached straight pipes is modeled with the length 20 times the mean radius r_m (see Figure 7A case a) to avoid end effects of the boundary conditions on the 90° curved hose. Our investigation confirms the selection of case a, to avoid boundary condition influence. In Figure 8B one sees, that the straight hose length and so the boundary conditions does not influence the radial stresses σ_r at the

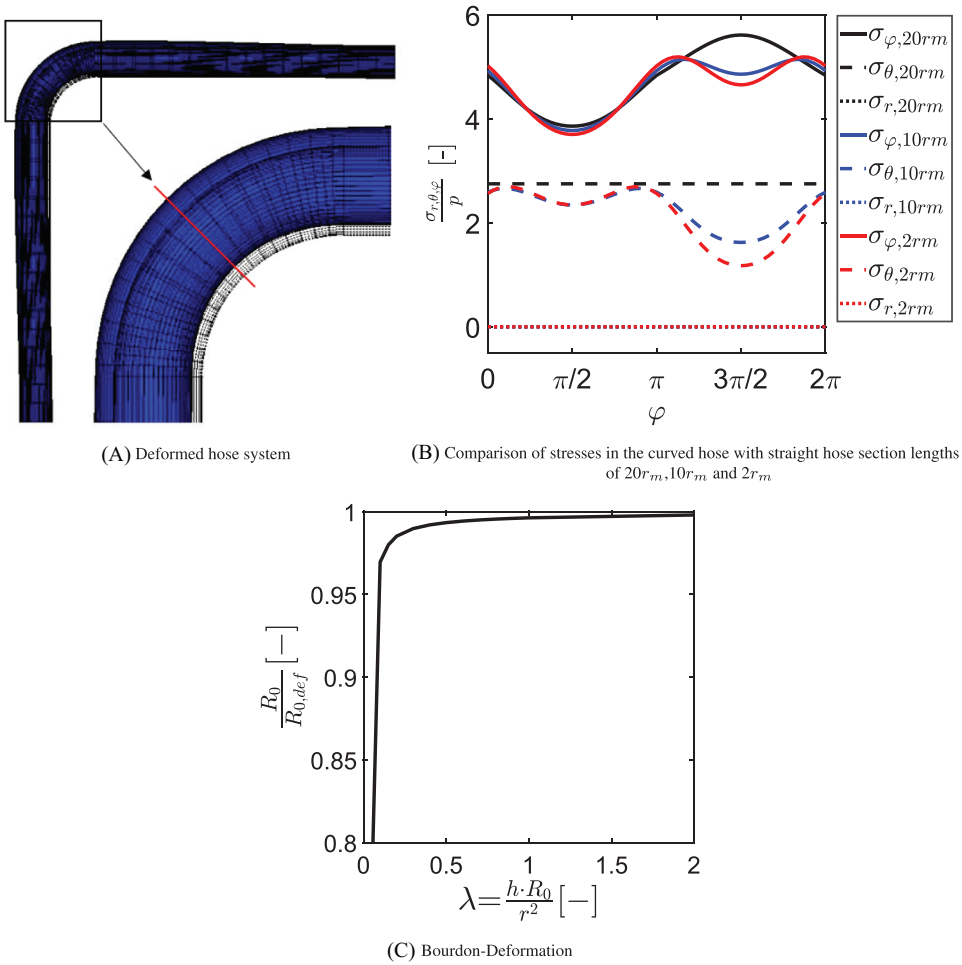

(A) Deformed hose system

(B) Comparison of stresses in the curved hose with straight hose section lengths of $20r_m$,$10r_m$ and $2r_m$

(C) Bourdon-Deformation

FIGURE 8 Combination of curved and straight hoses.

bend. But one observes a higher impact on the toroidal stresses σ_θ (blue and red dashed line) and on the poloidal stresses σ_φ (blue and red solid line) in case b and case c. So the poloidal stresses σ_φ and the toroidal stresses σ_θ are sensible to boundary effects.

To compare the undeformed and deformed curvature radius $\frac{R_0}{R_{0,def}}$ and to describe the deformation of the bend, the geometrical parameters are varied. For the calculation of this factor, the rotation of the cross-section due to deformation is neglected. In Figure 8C, we have shown the Bourdon deformation in comparison to the Kármán-Factor λ. The narrower and thicker the curved hose, the higher the outward deformation and the lower the factor $\frac{R_0}{R_{0,def}}$ becomes.

5 | SUMMARY AND OUTLOOK

The Bourdon effect is the most dominant influence on the deformation behavior of curved, pressurized hoses with linear elastic, isotropic material. Hence, in this contribution, we investigated the influence of the Bourdon effect using the example of a full torus and a quarter torus. For a full torus, the Bourdon effect is expressed by the increase in the radius of curvature, while for a quarter torus the Bourdon effect is expressed by the fact that the curved hose tends to straighten under internal pressure. Additionally, an ovalization of the cross-section is observed in both examples, which is attributed to a non-constant poloidal stress, which was derived analytically for a full torus. The model of the quarter torus was extended by two straight hoses at both ends and the influence of the boundary conditions on the stress distribution and the influence of the geometrical parameters on the deformation behavior was shown. Our next step is to include fiber rein-

forcements into our simulations in order to get closer to the hose behavior of practical applications. Therefore, various modeling techniques are tested and described.

ACKNOWLEDGMENTS

Open access funding enabled and organized by Projekt DEAL.

ORCID

Quirin Hoesch https://orcid.org/0000-0001-6366-3547

REFERENCES

1. Linn, J., Schneider, F., Dreßler, K., & Hermanns, O. (2022). Virtual product development and digital validation in automotive industry. In H. G. Bock, K. H. Küfer, P. Maass, A. Milde, & V. Schulz (Eds.), *German success stories in industrial mathematics*. Mathematics in industry (pp. 45–52). Springer.
2. Linn, J., Hermansson, T., Andersson, F., & Schneider, F. (2017). Kinetic aspects of discrete cosserat rods based on the difference geometry of framed curves. *Proceedings of the 8th ECCOMAS Thematic Conference on Multibody Dynamics*, Czech Republic, (2017), 163–176.
3. Abdulhameed, D., Adeeb, S., Cheng, R., & Martens, M. (2016). The influence of the Bourdon effect on pipe elbow. *Proceedings of the 11th International Pipeline Conference*, Canada, (2016).
4. Göldner, H., & Holzweißig, F. (1976). *Leitfaden der technischen mechanik*. VEB Fachbuchverlag.
5. Bourdon, E. (1849). Notes on pressure gauges. (1849).
6. Thiagarajan, N. (2013). Estimation of pipe elbow anchor loads due to internal pressure. *International Journal of Engineering and Innovative Technology*, *2*, 314–317.
7. Von Kármán, T. (1911). Über die formänderung dünnwandiger rohre. Insbesondere federnder ausgleichsrohre. *Zeitschrift des Vereins deutscher Ingenieure*, *55*, 1889–1895.
8. Zienciewicz, O. C., Taylor, R. L., & Fox, D. D. (2013). *The finite element method for solid & structural mechanics*. Butterworth-Heinemann.
9. ANSYS Inc. Academic Research Mechanical, Release 22.2.
10. Matzen, V. T., & Yu, L. (1998). Elbow stress indices using finite element analysis. *Nuclear Engineering and Design*, *181*, 257–265.
11. Matzen, V. T., & Yu, L. (1999). B2 stress index for elbow analysis. *Nuclear Engineering and Design*, *192*, 261–270.
12. Shemirani, F., Adeeb, S., Cheng, R., & Martens, M. (2014). Investigation of the influence of the Bourdon effect on the stress and ovalization in elbows. *Proceedings of the 10th International Pipeline Conference*, Cananda, (2014).

How to cite this article: Hoesch, Q., Roller, M., Schneider-Jung, F., Linn, J., & Müller, R. (2024). Analysis and simulation of curved hoses under internal pressure—3D continuum models. *Proceedings in Applied Mathematics and Mechanics*, *24*, e202400112. https://doi.org/10.1002/pamm.202400112